Available online at www.sciencedirect.com

ScienceDirect

Acta Materialia 72 (2014) 148–158

Acta MATERIALIA

www.elsevier.com/locate/actamat

Sliding wear-induced chemical nanolayering in Cu–Ag, and its implications for high wear resistance

F. Ren [a], S.N. Arshad [a], P. Bellon [a,*], R.S. Averback [a], M. Pouryazdan [b,c], H. Hahn [b,c]

[a] Department of Materials Science and Engineering, University of Illinois at Urbana-Champaign, Urbana, IL 61801, USA
[b] Institute of Nanotechnology, Karlsruhe Institute of Technology, 76021 Karlsruhe, Germany
[c] Joint Research Laboratory Nanomaterials, Technische Universität Darmstadt, 64287 Darmstadt, Germany

Received 22 January 2014; accepted 29 March 2014

Abstract

Sliding friction of metallic materials results in severe plastic deformation of the contacting surfaces. While plastic deformation is generally considered detrimental, as it leads to localized material failure and wear, in some cases it can trigger the formation of self-organized microstructures with the potential for improved wear resistance. We report here on a novel, self-adapting mechanism in a $Cu_{90}Ag_{10}$ two-phase alloy that relies on the spontaneous formation of chemically nanolayered structures during sliding wear. For sufficiently large initial Ag precipitate sizes, the nanolayered structures remain stable up to the sliding surface, leading to a reduction in wear rate. Similar chemically nanolayered structures are observed in $Cu_{90}Ag_{10}$ alloys deformed by high-pressure torsion, enabling controlled investigation of this process. The results of these studies suggest a novel approach, through self-organization, for designing metallic alloys that can achieve low wear rates.

Keywords: Copper alloys; Wear; Deformation structures; Self-organization and patterning; High-pressure torsion

1. Introduction

Wear-resistant materials are traditionally designed by engineering bulk materials and coatings to achieve either low shear strength or high hardness. Babbitt bearing alloys are examples of the former case, while hardfacing materials such as Stellite alloys illustrate the latter. High hardness can conveniently be achieved by reducing the grain size of the materials of interest. For example, it has been recently recognized that preparing or processing materials by severe plastic deformation (SPD) makes it possible to reduce grain sizes to a few tens of nanometers, thus reaching strength levels that approach theoretical limits [1–5]. In two-phase alloys, moreover, SPD can also result in highly non-equilibrium morphologies that are not readily achieved by other means [6–8]. Materials evolving during wear generally undergo SPD just below the sliding surface. This suggests an approach for the design of wear-resistant materials that exploits the mechano-chemical processes induced by friction and wear to generate unique surface and subsurface structures that provide wear resistance. The non-linear character of friction [9], combined with the microstructural evolutions induced by SPD [2,10], can generate positive feedback loops, thus providing opportunities to design self-adapting materials.

A well-known example of self-adaptation during wear is the spontaneous formation of tribolayers, so-called "third bodies" [11], which act as solid lubricants [10,12–14]. In "chameleon" coatings [15], for example, friction induces a transition from sp^3 to sp^2 bonding in diamond-like carbon atoms, resulting in a reduction of friction and wear. Recent

* Corresponding author. Tel.: +1 (217) 265 0284; fax: +1 (217) 333 2736.
E-mail address: bellon@illinois.edu (P. Bellon).

http://dx.doi.org/10.1016/j.actamat.2014.03.060
1359-6454/

atomistic simulations of diamond–diamond sliding revealed that this sp^3-to-sp^2 transition was accompanied by the formation of a lubricious amorphous tribomaterial [16]. The benefits of tribolayers can be extended further by tailoring coating compositions so that distinct lubricious tribolayers form under different operating conditions [17,18], making it possible to achieve very low friction and wear over a broad range of temperature, humidity and surface chemistries, including those involving oxidative environments [19,20]. Processes taking place below the sliding surface can also be beneficial. In Ni–W nanograined coatings, for instance, sliding-induced chemical and microstructural relaxations at grain boundaries increase hardness in the wear track, reducing the wear rate [21,22]. Beyond these accomplishments, the opportunities afforded by self-adaptation for the design of wear-resistant materials remain vast and largely unexplored.

In the present work, we report on a novel morphology driven by SPD during sliding wear in two-phase materials. The self-organization process reported here for $Cu_{90}Ag_{10}$ alloys leads to the formation of alternating Cu-rich and Ag-rich nanolayers with thicknesses decreasing progressively to a few nanometers as the sliding surface is approached. As we will show, these nanolayers provide excellent wear resistance. Using thermal annealing to control the size of the initial Ag precipitates before exposure to sliding wear, the thickness of the nanolayers at the surface can be easily controlled. For too small precipitates, the layers dissolve into a homogeneous alloy, and wear resistance decreases. We thus find that the initial length scale of the precipitate structure has a profound influence on the microstructures evolved during wear and accordingly on the wear rates. The larger the Ag precipitates are, the lower the wear rates, despite the fact that larger Ag precipitates also translate into softer materials. It is proposed that the presence of Ag nanolayers just below the wear surface is the key microstructural feature responsible for the observed reduction in wear rate. Selected $Cu_{90}Ag_{10}$ samples were also deformed by high-pressure torsion (HPT), and similar chemical nanolayering was observed for a range of plastic strains, thus providing a basis for controlling this phenomenon. We conclude that wear-induced chemical nanolayering can be controlled by adjusting alloy chemistry and initial microstructure. The present results therefore offer a promising broad approach for designing wear-resistant materials.

2. Methods

2.1. Fabrication of two-phase $Cu_{90}Ag_{10}$ alloys

Commercially pure copper and silver powders were combined to obtain an average molar composition of 90% Cu and 10% Ag and then subjected to high-energy ball milling using a SPEX 8000 mill in an argon glove box for 12 h at ambient temperature (~50 °C). Ball milling forces the mixing of Cu and Ag into a solid solution [23]. The ball-milled powders were then compacted by warm pressing at 300 °C with a 1 GPa load under high vacuum (2×10^{-6} Pa), producing cylinders with density exceeding 99% of the theoretical density. During sintering, Ag precipitated into nearly equiaxed precipitates, with a volume-averaged diameter of 32 nm, as determined by scanning transmission electron microscopy (STEM) [24]. Some of these samples were further annealed at 450, 600 and 750 °C for 1 h in an argon tube furnace, leading to volume-averaged precipitate diameters of 58, 122 and 262 nm, respectively [24], as illustrated in Fig. 1. A limited contamination of powders during ball milling by milling tools led to the formation of small Fe_2O_3-type precipitates during compaction and annealing. The size and density of these nanoscale precipitates, which are easily detected by Z-contrast imaging (see e.g. the arrows in Fig. 1), did not vary much over the range of annealing temperatures investigated here, as illustrated by the histograms in Fig. S1. Their contribution to the variation of wear response with the initial Ag precipitate size should therefore be minimal. Lastly, hardness, measured by nanoindentation, decreased from 5.2 GPa for the as-compacted samples to 2.5 GPa for the highest annealing temperature, 750 °C (see Table 1).

2.2. Wear testing

Pin-on-disk wear tests were performed in air under 1 kgf load (~1.38 MPa nominal pressure) using either a martensitic stainless steel 440C disk or a Cu–Ni–Sn bronze disk as the counterface material, using a procedure similar to the one described in detail in Refs. [13,25]. A sliding velocity of 0.25 m s^{-1} was selected to suppress flash heating at the contacting surfaces, and local pin temperature measurements yielded temperatures between 60 and 70 °C. Continuous measurements of the pin displacement and of the frictional force established that wear had reached a steady state when sliding distances exceeded ~60 m. Steady-state wear rates were calculated by weight loss measurements after sliding distances of 450 m. Prior to wear testing, the contacting surfaces of the sample and disk were mechanically polished to achieve an average surface roughness (R_a) of less than 200 nm, as measured by a Sloan Dektak^3 ST stylus surface profilometer. Three separate tests were run for each specimen, and the average wear rates and coefficients of friction are reported in Table 1.

2.3. Microstructural and mechanical characterization

The microstructures of the worn samples were characterized by TEM and STEM, including high-angle annular dark field (HAADF) imaging and energy-dispersive spectroscopy (EDS), using JEOL 2010 TEM and STEM microscopes operated at 200 kV. The directions normal to the sliding surface, along the sliding direction and perpendicular to the sliding direction in the sliding plane were defined as ND, SD and TD, respectively. ND–SD and ND–TD cross-sectional TEM samples were prepared

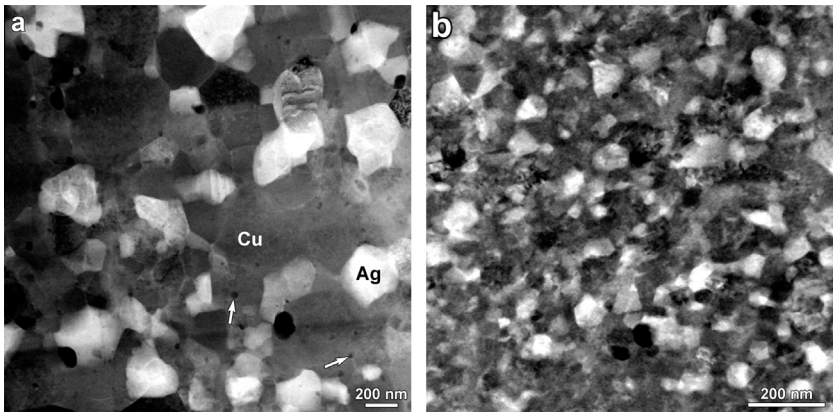

Fig. 1. HAADF-STEM images of the as-synthesized two-phase $Cu_{90}Ag_{10}$ alloys, after annealing at (a) 750 °C and (b) 450 °C. Ag-rich precipitates appear brighter than the matrix, while small Fe_2O_3 particles (pointed out by arrows), due to contamination during ball milling, are darker than the matrix.

Table 1
Effect of heat treatment on average Ag precipitate diameter (nm), hardness (GPa), coefficient of friction (COF, dimensionless) and wear rate ($mm^3\ N^{-1}\ m^{-1}$) for two-phase $Cu_{90}Ag_{10}$ alloys worn against SS440C stainless steel and Cu–Ni–Sn bronze disk.

Annealing temperature (°C)	Precipitate diameter	Hardness	COF	Wear rate	COF	Wear rate
			SS 440C		Cu–Ni–Sn	
As pressed	32	5.2	0.64	1.70×10^{-5}	0.57	2.33×10^{-4}
450	58	4.2	0.63	1.49×10^{-5}	0.52	1.38×10^{-4}
600	122	3.1	0.67	1.28×10^{-5}	0.51	8.64×10^{-5}
750	262	2.5	0.64	9.12×10^{-6}	0.50	1.42×10^{-5}

by focused ion beam (FIB; FEI Strata 235 and Helios NanoLab™ 600i) milling using the standard lift-out technique. A protective platinum strip of thickness ~1 μm was deposited on the worn surface before the FIB milling. Nanoindentation was performed using a Hysitron TI-950 Triboindenter on mechanically polished cross-sections of the pins to determine the hardness as a function of depth in the worn samples. For each indentation mark, the distance to the wear surface was directly measured using SEM images to minimize errors due to the large surface roughness. Note also that the presence of the worn surface edge made it impossible to obtain reliable data for depths less than ~1 μm below the wear surface. The morphologies of the pin surfaces were also analyzed by scanning electron microscopy (SEM), and the wear debris characterized by SEM and TEM.

3. Results

3.1. Wear performances and microstructures

The surface morphologies of all worn pins show features characteristic of strong adhesive wear, regardless of the counterface material used as the disk during the wear tests. The coefficients of friction, ~0.5 for the Cu–Ni–Sn disk and ~0.65 for the SS 440C disk, are typical values for dry sliding of metallic materials [26]. The wear debris comprised nearly equiaxed particles a few microns in size for the SS 440C disk and flakes several hundred of microns in length for the Cu–Ni–Sn disk. These differences in debris size, as well as the lower wear rates for the SS440C counterface, are consistent with previous results [13] showing that a lubricious tribolayer formed at the pin/disk interface for the SS440C counterface. For both counterface materials, however, wear rates were observed to vary significantly with the initial Ag precipitate size, in a way that could not be simply accounted for by the appearance of the worn surfaces and the analysis of the wear debris. We thus carried out a detailed characterization of the pin microstructures in steady-state wear.

One remarkable result of the wear data is that the softer alloys exhibit a lower wear rate, in contradiction with the commonly observed correlation between wear resistance and hardness, as captured in Archard's law [27]. This unexpected result correlates with distinct microstructures near the wear surface. We first describe the worn microstructure for the alloy with the largest initial Ag precipitate size, $d_p = 262$ nm. Crystalline nanolayers are clearly observed below the wear surface, and electron diffraction patterns indicate that two face-centered cubic (fcc) phases are present (see Fig. 2). HAADF-STEM imaging reveals the presence of alternating high-Z and low-Z nanolayers in ND–SD cross-sections, as illustrated in Fig. 3. The spacing between the Ag-rich nanolayers increases nearly linearly with the distance below the sliding surface, as seen in Fig. 4. The compositions of the brighter (higher-Z) and darker (lower-Z) layers, measured by STEM–EDS at ~1.8 μm below the sliding surface, were ~$Cu_{18}Ag_{82}$ and $Cu_{98.5}Ag_{1.5}$, respectively. These compositions are very close to those of the phases present in the initial microstructure,

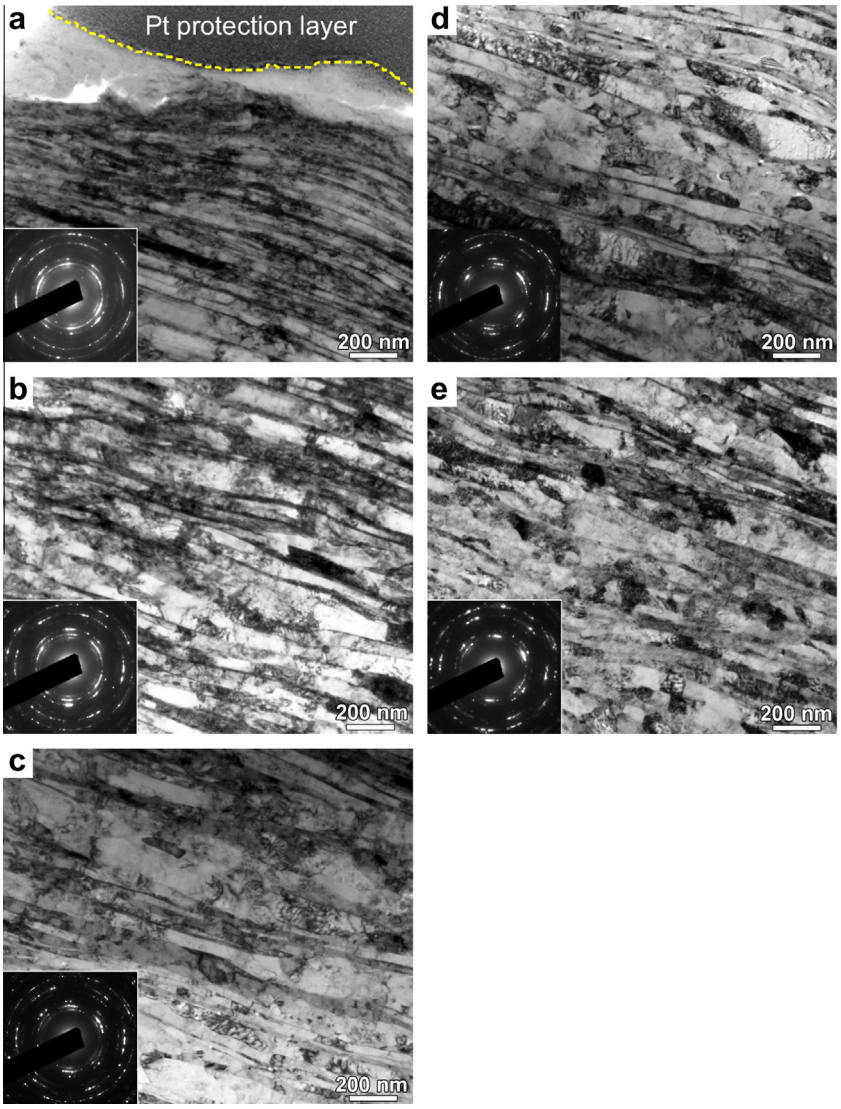

Fig. 2. Bright-field TEM images and diffraction patterns at various depths below the sliding surface of $Cu_{90}Ag_{10}$ alloy annealed at 750 °C ($d_p = 262$ nm) and worn against SS 440C disk. (a) $d = 0$–1 μm; (b) $d = 1$–2.5 μm; (c) $d = 2.5$–4 μm; (d) $d = 4$–5.5 μm; and (e) $d = 5.5$–7 μm. Each area overlaps slightly with the previous one (see also Fig. 3).

suggesting that the nanolayers formed by co-deformation with little atomic mixing. Note that the rather large Cu content in the Ag-rich initial precipitates is consistent with the 14.1 at.% equilibrium solubility of Cu in Ag at the eutectic temperature of 779 °C. At a depth beyond ~6 μm, the chemically layered structure becomes progressively replaced by a microstructure that is increasingly similar to the initial one, with large and nearly equiaxed Ag-rich precipitates.

The main material flow direction imposed by the present wear testing is along SD, and this is consistent with the overall morphological evolution of the Ag and Cu phases observed in ND–SD cross-sections (see Figs. 2 and 3). It is observed, however, that the Ag precipitates are deformed significantly along TD as well as along SD, as illustrated on an ND–TD cross-section in Fig. 5 (see also Fig. S2 for the microstructure as a function of the depth below the wear surface). The length of the Ag layers just below the wear surface approaches ~1 μm along TD, whereas the typical layer length along SD exceeds 2 μm. The morphology of the precipitates before they form continuous nanolayers provides a useful insight into the mechanisms involved in the nanolayering reaction. As seen in Fig. 5, pairs of bright-field TEM and HAADF-STEM images from ND–TD cross-sections, here observed ~1.5 μm below the wear surface, reveal that the Ag precipitates deform along Cu grain boundaries, with the stretched tips of the precipitates ending either within Cu grains (see e.g. arrow A in Fig. 5) or at Cu/Cu boundaries (see e.g. arrow B in Fig. 5). One also notices that many Cu/Cu grain boundaries elongated along TD are yet not decorated by any Ag precipitates (see e.g. arrow C in Fig. 5). These results suggest that the plastic deformation and stretching of the Ag precipitates is guided by Cu/Cu grain boundaries, as will be discussed in the next section.

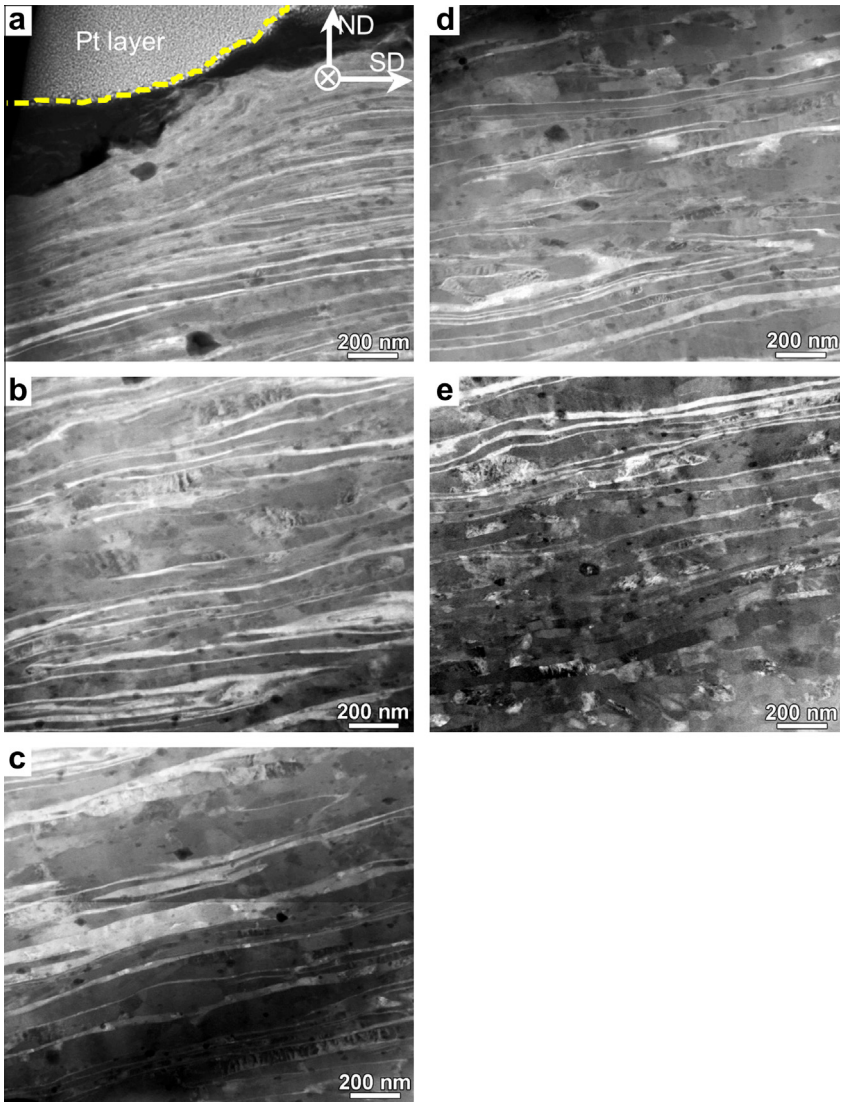

Fig. 3. HAADF-STEM images of the same areas shown in Fig. 2.

The worn microstructures were significantly different when the starting $Cu_{90}Ag_{10}$ material had a smaller initial precipitate size. For samples annealed at 450 °C, which resulted in an initial precipitate diameter of $d_p = 58$ nm, the worn microstructure comprised three regions, as illustrated in Fig. 6(a and b). In the topmost region, extending from the wear surface to a depth of ~600 nm, only a single phase Cu–Ag solid solution was present, as indicated by the presence of just one fcc phase in the diffraction patterns (Fig. 6(a)) and uniform Z contrast (Fig. 6(b)). The composition of the solid solution is found by STEM–EDS to be $Cu_{88.5}Ag_{11.5}$, in agreement with the lattice parameter of 0.372 nm determined from the diffraction patterns [28]. This composition is very close to that of the initial alloy. Furthermore, grains in this solid solution were equiaxed. Below this solid solution layer, and extending over ~500 nm, was a chemically layered structure similar to the ones observed just below the wear surface in the material annealed at 750 °C. At greater depths, i.e. in the third region, a microstructure with individual Ag-rich precipitates was recovered, with the precipitates becoming more and more equiaxed with increasing depth. A very similar microstructure, with three distinct regions, was observed for the as-pressed samples (see Figs. S3 and S4). In contrast, for the samples annealed at 600 °C, chemical nanolayering extends all the way to the sliding surface (see Fig. S5), as for the samples annealed at 750 °C.

The evolution of sample hardness below the sliding surface was measured using nanoindentation on polished cross-sections. In order to avoid any potential interaction between the plastic zones of the individual intents, the successive indents were shifted from the previous one by 10 μm along x (TD), and 0.5 or 1 μm along y (ND), as illustrated in Fig. 7a. As expected, the microstructural refinement imposed by wear correlates with a gradual increase in hardness, for both $d_p = 58$ nm and $d_p = 262$ nm, with maximum values of 5.1 and 3.3 GPa, respectively (see Fig. 7). These hardness profiles are similar to ones reported for worn

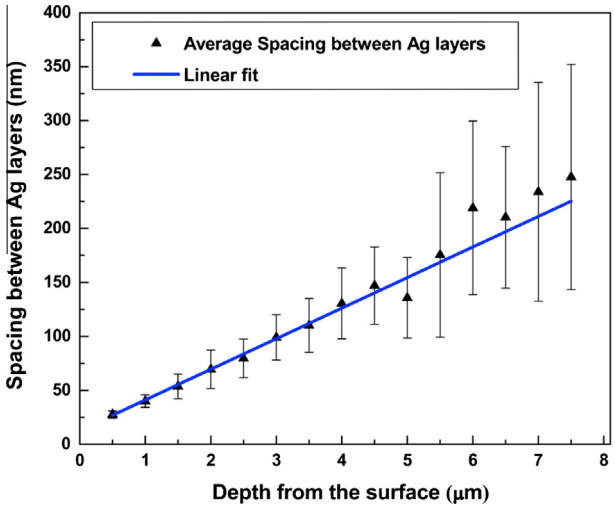

Fig. 4. The spacing between two consecutive Ag layers as a function of depth below the sliding surface for $Cu_{90}Ag_{10}$ alloy annealed at 750 °C and worn against SS440C disk. Error bars correspond to one standard deviation from 15 measurements for each depth.

Cu–Ag eutectic alloys [25]. It is of note that the maximum hardness of the $d_p = 262$ nm sample, 3.3 GPa, is lower than the base hardness of the $d_p = 58$ nm sample, 4.2 GPa, and significantly lower than its maximum hardness, 5.1 GPa. Therefore, the improved wear resistance observed in the Cu–Ag alloys with large initial Ag precipitate size cannot result from deformation-induced hardening.

3.2. High-pressure torsion microstructures

In order to confirm that the nanolayering was induced by the deformation imposed by sliding wear, we subjected samples from the same $Cu_{90}Ag_{10}$ materials to HPT. Room-temperature HPT has indeed been shown to force Cu and Ag into solution, starting from hypoeutectic alloys [29], eutectic alloys [30] or Ag precipitates in a Cu matrix [24]. While other SPD techniques, such as high-energy ball milling of elemental powders, can also force the moderately immiscible elements Cu and Ag into solid solution [8,23,31–37], an important advantage of HPT is that shear strain γ can be quantified using the expression $\gamma = 2\pi r\Delta\theta/t$, where t is the specimen thickness, $\Delta\theta$ is the angle of rotation and r is the radial distance from the torsion axis. This equation assumes that the deformation is homogeneous throughout the sample thickness [7,38]. Additionally, the predominant deformation mode during HPT is nearly simple shear, as is the case for sliding wear, although other modes can also be present close to the wear surface, owing to the triaxial stress state in contacting asperities [39].

Cu–Ag disks with initial precipitate size $d_p = 262$ nm were deformed by HPT using the procedure detailed by Arshad et al. [24], except that we used continuous torsion in one direction so as to better simulate sliding wear. Cross-sectional TEM samples were prepared at radial distances from the torsion axis corresponding to shear strains of ≈60 and 120. TEM and HAADF-STEM analyses indicate that the HPT microstructures were very similar to the ones observed in worn samples, and in particular chemical nanolayering was also observed in the HPT samples, as illustrated in Fig. 8. The average distances between two consecutive Ag layers were 22.9 ± 4.2 and 18.1 ± 2.3 nm, for the samples deformed by HPT to strains of ~60 and 120, respectively. The layer thickness for the latter strain is close to the value of ~15 nm obtained by extrapolating up to the wear surface measurements made below it (see Fig. 4). This suggests that the maximum strain in worn samples exceeds slightly ~120. We note that wear-induced layering appears to stabilize layers that are more regular than the ones induced by HPT (compare e.g. Fig. 3(a) with Fig. 8(a and b)). The HPT layers are rougher, and sometimes exhibit kinks. Whether this difference is an effect of a nearby surface in the one case but not the other, or is a somewhat different strain path, is currently under investigation.

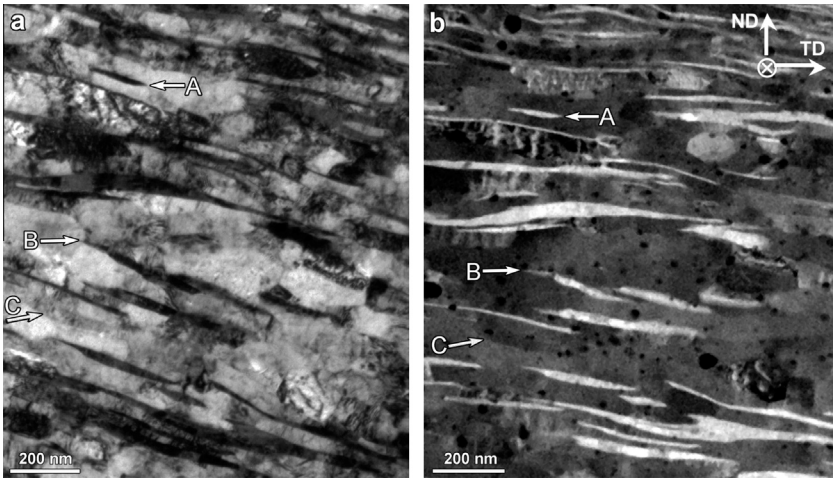

Fig. 5. ND–TD cross-section of two-phase $Cu_{90}Ag_{10}$ alloy annealed at 750 °C and worn against SS 440C disk: (a) bright-field TEM image and (b) corresponding HAADF-STEM image, ~1.5 μm below the wear surface. Arrows A and B point to Ag precipitate tips ending in Cu grains and at Cu/Cu boundaries, respectively. Arrow C points to Cu/Cu grain boundaries not separated by Ag layers.

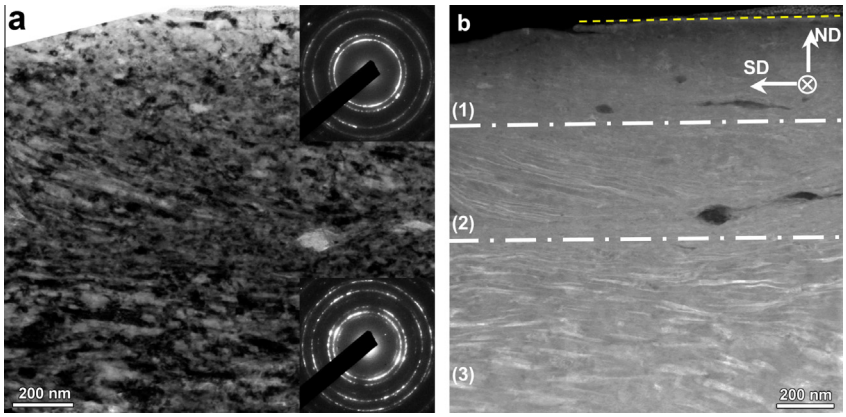

Fig. 6. ND–SD cross-section of $Cu_{90}Ag_{10}$ alloy annealed at 450 °C and worn against SS 440C disk: (a) bright-field TEM image and (b) corresponding HAADF-STEM image just below the wear surface (yellow dashed line). Three regions are identified: (1) Cu–Ag solid solution; (2) Cu–Ag nanolayered structures; and (3) deformed bulk two-phase Cu–Ag. (For interpretation of the references to color in this figure legend, the reader is referred to the web version of this article.)

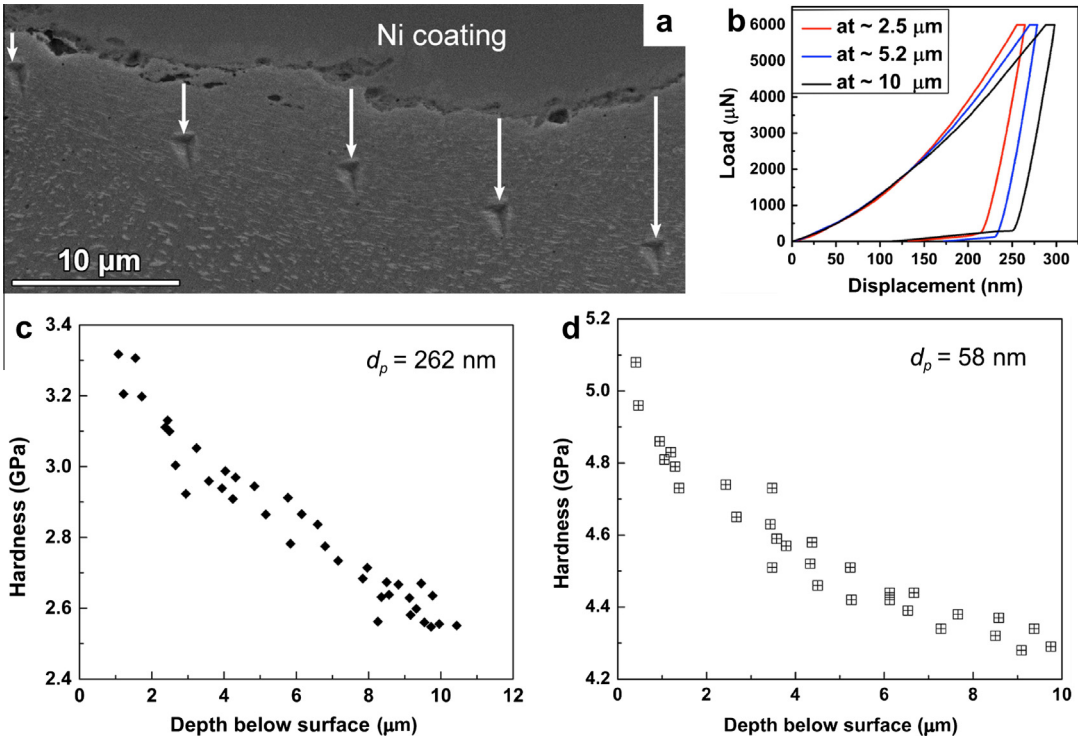

Fig. 7. (a) ND–TD cross-sectional SEM image with indentation marks, (b) load–displacement curves at different depths and (c and d) hardness changes with depth below wear surface for different initial precipitate diameters, d_p. Note that (a) and (b) are from the sample with $d_p = 262$ nm. Electroless Ni coating was applied after wear to protect the surface during cross-section polishing.

The recent HPT investigations of forced chemical mixing in Cu–Ag explain why a solid solution formed just below the wear surface in the case of initial Ag precipitate size of $d_p = 58$ nm (Fig. 6(a and b)), while a two-phase microstructure was retained for samples with $d_p = 262$ nm (Figs. 2(a) and 3(a)). Indeed Arshad et al. [24] found that the strain needed to achieve a solid solution, ε_{mix}, scaled linearly with the size of the Ag precipitates, from $\varepsilon_{mix} \sim 110$ for $d_p = 58$ nm to $\varepsilon_{mix} \sim 700$ for $d_p = 262$ nm, in good agreement with a theoretical prediction based on the superdiffusive character of the chemical mixing forced by plastic deformation [36,40]. If we assume that the maximum shear strain reached during sliding wear, just below the wear surface, is the same for samples with $d_p = 58$ nm and $d_p = 262$ nm, the above HPT results on mixing suggest then that this maximum strain is larger than 100 but less than 700. This estimate is compatible with the one derived in the previous paragraph from the comparative analysis of the chemical layer thickness in worn and HPT samples. While this estimate for the shear strain at the wear surface

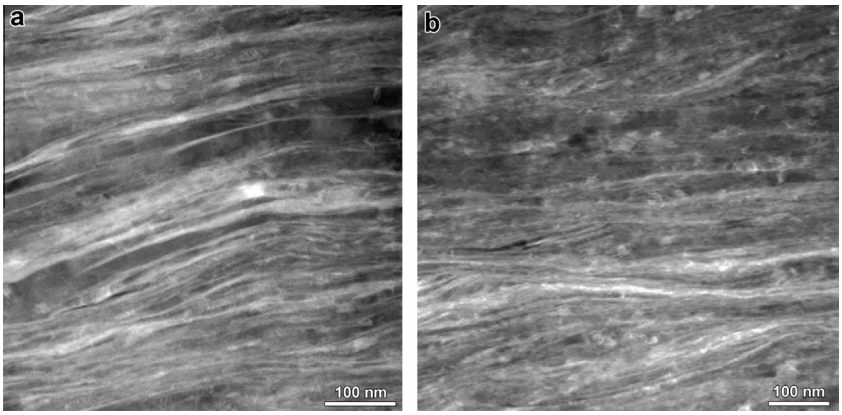

Fig. 8. HAADF-STEM images on ND–SD cross-section of $Cu_{90}Ag_{10}$ alloy annealed at 750 °C and subjected to HPT to a shear strain of (a) ~60 and (b) ~120. Chemical nanolayering is observed in both cases.

is large, it is compatible with measurements obtained on other metallic tribopairs [10,13,41]. Note that the methods traditionally used to estimate shear strains induced by wear are not applicable here, because the small initial grain size and the precipitate dissolution preclude the use of fiducial markers, such as grain boundaries [10,41] or layer rotation in eutectics [25].

4. Discussion

The microstructural characterization of the worn layers suggests that the improvement in wear resistance is due to the presence of Ag nanolayers just below the sliding surface. This rationalization derives from the well-established practice of using soft metal coatings, such as Babbitt alloys, to localize plastic deformation in these surface layers, thereby reducing wear. Ag is in fact commonly used as a solid lubricant at moderate temperatures, ranging from room temperature to ~500 °C. TEM diffraction patterns suggest that the nanolayers develop a shear texture, with ⟨1 1 1⟩//ND, which is typical of fcc metals. This texture should further facilitate shear localization in the Ag layers or, more likely, at the Cu/Ag interfaces, just below the wear surface. It should be noted that the reduction in wear rate is largest, by a factor of about 20, when a Cu–Ni–Sn bronze is used as the counterface disk for wear testing (see Table 1). In this case, no tribolayer is observed at the sliding surface. In contrast, when the counterface material is SS440C, a well-defined tribolayer develops, comprising a mixture of nanocrystalline metallic Cu and Ag-rich phases, as well as Cu-based and Fe-based oxides (see Figs. S6 and S7 in Supplemental information). These observations are in agreement with prior results on tribolayers [13,42]. It was found in those studies that when SS440C is used as the counterface material the tribolayer acted as a lubricant and reduced wear. It is therefore not surprising that the improvement brought about by chemical nanolayering is smaller in this case. The important conclusion here is that tribolayers cannot explain the measured reductions in wear rate with the initial Ag precipitate size since (i) they are present with similar characteristics for all pin-on-disk experiments performed against SS440C disk and (ii) they are absent in the case of tests performed against Cu–Ni–Sn disk.

The main distinctive difference between the different worn microstructures resides in the spatial extension of the Ag and Cu nanolayers. The nanolayering observed here in Cu–Ag is reminiscent of the crystallographic nanolayering reported by Hughes et al. in pure metals like Cu, Al and Ni subjected to severe plastic deformation [43–46]. In both cases, large equiaxed grains are transformed into layers whose thickness decreases as strain increases. The dependence of the layer thickness with depth below the wear surface for Cu–Ag (Fig. 4) is remarkably similar to the measurements reported in Ref. [45] for Cu subjected to a friction test. In both cases, the thickness of individual layers decreases approximately linearly upon approaching the sliding surface, reaching a minimum value of ~10 nm. In the case of crystallographic nanolayering, it has been established that the layers are separated by geometrically necessary boundaries (GNBs), the thickness and misorientation dependence with strain of which obey a similitude principle [45]. These features have been rationalized by local imbalances in slip system activity in materials undergoing stage III and IV dynamical recovery [47–50]. Very recently, surface mechanical grinding treatment of pure Ni at a high strain rate has also been reported to produce a nanolayered structure in pure Ni that is remarkably stable during annealing [51]. These previous results were obtained on pure elements or single-phase material, and thus one important novel result of the present work is the stabilization by severe plastic deformation of alternating Cu-rich and Ag-rich nanolayers. This self-organization results from a complex evolution of the microstructure of this two-phase alloy. In fact, recent experiments on nanoscale Ag–Cu eutectic alloys subjected to surface mechanical attrition treatment (SMAT) showed that the pre-existing Cu layers were destabilized and progressively transformed to smaller Cu precipitates [52]. In contrast, in our experiments, the morphology of the Ag-rich phase is transformed from

initially equiaxed precipitates to platelets stretched along the SD direction, as well as along the TD direction, as seen in Figs. 3 and S2. Observations made at intermediate strains, before these platelets form nearly continuous layers (see Fig. 5), reveal that the platelet tips are frequently located at Cu/Cu layer boundaries. We thus propose that the chemical layering results from the plastic deformation and stretching of Ag precipitates guided by GNBs that progressively form in the matrix as the strain increases, as they would in pure Cu. The layer thickness should thus largely be determined by the crystallographic layering of the Cu matrix. This rationalization suggests that it should be enlightening to characterize the Cu/Ag and Cu/Cu boundaries in the nanolayering regime, and in particular the orientation relationships of these boundaries. This is left for future work. As Cu–Ag eutectic layers are destabilized during SMAT, we conclude that the deformation mode, which is predominantly simple shear in sliding wear and in HPT but not during SMAT, plays an essential role in chemical nanolayering.

It is important to note that, while chemical nanolayering is a transient phenomenon in samples processed by HPT, it may be permanently present at the wear surface under steady-state wear. When plastic strain can be indefinitely increased, e.g. in ball milling or HPT, room-temperature plastic deformation always leads to the homogenization of Cu–Ag alloys. In these cases, nanolayering is a transient microstructure. For sliding wear, however, the system imposes a boundary condition not found for ball milling and HPT. Specifically, strain is not an independent variable, and steady-state wear regimes are reached for a finite maximum strain of the pin material, as surface material is continuously removed, forming wear debris. It is therefore possible to maintain in steady-state wear a surface that is permanently self-organized into chemically alternating nanolayers, provided that the maximum strain experienced by the material is less than the critical strain required for dissolution. In this work, we control the critical strain for dissolution by increasing the initial Ag precipitate size via annealing. If the initial precipitate size is too small, e.g. for the as-pressed samples or the samples annealed at 450 °C, the maximum strain at the wear surface exceeds the critical strain, resulting in a solid solution at the wear surface and inferior wear resistance. When the initial precipitate size is large enough, as in the case of samples annealed at 600 and 750 °C, the maximum strain at the sliding surface is less than the critical strain and alternating Ag and Cu nanolayers are thus permanently present at the sliding surface in steady-state wear.

Deformation-induced chemical nanolayering, and its associated reduction in wear rate, should be observable in other alloy systems. The prerequisites are that the starting microstructure of these alloys would contain precipitates of either low melting point and ductile metals, such as Ag, Sn, In or Bi, or other low shear strength phases that could initially co-deform with the matrix, until forming near continuous layers. Plastic deformation near the wear surface should then localize in these layers, resulting in a reduction of wear rate. The initial precipitates should be sufficiently small to form nanolayers during wear up to the sliding surface, but large enough not to homogenize. While some chemical nanolayering is also observed for samples with small initial precipitate diameters (see regions 2 in Figs. 6 and S3), this nanolayering does not extend all the way up to the wear surface and therefore cannot lubricate contact asperities. It is interesting to compare the present results with the approaches employed for the design of "chameleon" coatings [15,17,18,53], where sliding wear of a composite material leads to the coating of the wear surface with lubricious phases such as Ag, Mo oxides and silver molybdates. An essential difference is that, in this last approach, thermal activation is necessary to promote the segregation of Ag or the formation of the oxides at the sliding surface, thus requiring elevated temperatures, ranging from 300 to 700 °C. Our work shows that wear-induced nanolayering reactions provide an alternative way to obtain extended layers reducing wear rates, even at temperatures at which thermal transport is limited. It should be interesting to investigate the effect of wear temperature on nanolayering in Cu–Ag since, at elevated temperature, thermally activated diffusion should promote layer and precipitate coarsening, thus possibly interfering with the stabilization of chemically distinct nanolayers. Experiments at low temperatures ($T < 50$ °C), on the other hand, should indicate whether diffusion plays any significant role in the novel self organization reaction reported in the present work. It will also be interesting to investigate chemical nanolayering in highly immiscible alloy systems, such as Ni–Ag, Fe–Ag or Cu–Nb, with heats of mixing in excess of 25 kJ mol^{-1}. Unlike Cu–Ag, which is only moderately immiscible with a heat of mixing ~6 kJ mol^{-1}, severe plastic deformation cannot force the stabilization of concentrated solid solutions in these alloy systems, and one can thus anticipate that, if chemical nanolayering takes place, it should persist up to the sliding surface regardless of the initial precipitate size. An important practical consequence would be that wear performance should then be much less sensitive to the initial alloy microstructure.

The potential benefits of severe plastic deformation for improving materials properties has now been recognized for more than a decade [2]. The emphasis of past studies, however, has been on elemental or single-phase materials. Recent works on two-phase materials have revealed novel possibilities, as illustrated, for instance, by the controlled stabilization of Cu–Nb nanolaminates with remarkable thermal stability by accumulative roll bonding [54]. In that case, the layered morphology was preserved throughout the repeated rolling of the material, starting from pure Cu and Nb sheets. It is anticipated that additional complex and functional self-organized nanostructures can be obtained by varying the strain path and alloy chemistry. An additional characteristic of wear-induced self-organized nanostructures is that they are graded, here over several microns, owing to the concentration of deformation near

the sliding surface. It would be interesting to investigate specifically the contribution of this grading, since graded microstructures can afford increased resistance to materials damage and failure [55]. The present work is encouraging toward these directions, already showing the beneficial effect of chemical layering that occurs spontaneously during SPD.

5. Conclusion

Dry sliding wear was observed to result in the spontaneous stabilization of chemical nanolayering in $Cu_{90}Ag_{10}$ two-phase alloys. The initial size of the equiaxed Ag-rich precipitates, which was controlled by annealing prior to wear testing, was found to have a profound impact on worn microstructures and wear performances. For large enough initial diameters, 122 and 262 nm in the present study, alternatingly Ag-rich and Cu-rich nanolayers were present several microns below, and up to, the sliding surface during steady-state wear. In contrast, for smaller initial Ag precipitate diameters, 32 and 58 nm, the mixing forced by plastic deformation lead to the stabilization of a nanocrystalline Cu–Ag solid solution just below the sliding surface. TEM revealed that, for large enough initial Ag precipitates, wear-induced plastic deformation led to the stretching of the initially equiaxed precipitates along both the sliding direction and the transverse direction, resulting in the formation of nanolayers extending over 1 μm in the sliding plane. It is proposed that the stretching of the Ag precipitates into layers was guided by the GNBs formed in the Cu matrix during wear. Similar alternating layers were also found when the same alloys were subjected to SPD by HPT, which, as sliding wear, imposes a predominantly simple shear deformation mode. Lastly, while the hardness of the alloys decreased as the initial Ag precipitate diameter increased, their wear rates decreased by a factor of 2–20. This unusual effect was explained by the ability of the Ag-rich nanolayers, when present up to the sliding surface, to lubricate sliding contacts. It is proposed that sliding wear-induced chemical nanolayering offers a novel strategy for the design of materials with high wear resistance.

Acknowledgements

This research was supported by the NSF under Grants DMR 09-06703, DMR 10-05813, and MRI 0923428. The work was carried out in part in the Frederick Seitz Materials Research Laboratory Central Facilities, University of Illinois, which are partially supported by the U.S. Department of Energy under Grants DE-FG02-07ER46453 and DE-FG02-07ER46471.

Appendix A. Supplementary material

Supplementary data associated with this article can be found, in the online version, at http://dx.doi.org/10.1016/j.actamat.2014.03.060.

References

[1] Hansen N, Mehl RF. Metall Mater Trans A 2001;32:2917.
[2] Valiev R. Nat Mater 2004;3:511.
[3] Valiev RZ, Alexandrov IV. Nanostruct Mater 1999;12:35.
[4] Tao NR, Sui ML, Lu J, Lua K. Nanostruct Mater 1999;11:433.
[5] Zhang YS, Han Z, Wang K, Lu K. Wear 2006;260:942.
[6] Bellon P, Averback RS. Phys Rev Lett 1995;74:1819.
[7] Cao Y, Wang YB, Alhajeri SN, Liao XZ, Zheng WL, Ringer SP, et al. J Mater Sci 2010;45:765.
[8] Suryanarayana C. Prog Mater Sci 2001;46:1.
[9] Urbakh M, Klafter J, Gourdon D, Israelachvili J. Nature 2004;430:525.
[10] Rigney DA. Wear 2000;245:1.
[11] Godet M. Wear 1984;100:437.
[12] Erdemir A, Li SH, Jin YS. Int J Mol Sci 2005;6:203.
[13] Singh JB, Wen JG, Bellon P. Acta Mater 2008;56:3053.
[14] Scharf TW, Prasad SV. J Mater Sci 2013;48:511.
[15] Voevodin AA, Zabinski JS. Thin Solid Films 2000;370:223.
[16] Pastewka L, Moser S, Gumbsch P, Moseler M. Nat Mater 2011;10:34.
[17] Voevodin AA, Zabinski JS. Compos Sci Technol 2005;65:741.
[18] Muratore C, Voevodin AA, Hu JJ, Zabinski JS. Wear 2006;261:797.
[19] Franz R, Mitterer C. Surf Coat Technol 2013;228:1.
[20] Liu EY, Gao YM, Wang WZ, Zhang XL, Wang X, Yi GW, et al. Tribol Trans 2013;56:469.
[21] Rupert TJ, Schuh CA. Acta Mater 2010;58:4137.
[22] Rupert TJ, Cai WJ, Schuh CA. Wear 2013;298:120.
[23] Klassen T, Herr U, Averback RS. Acta Mater 1997;45:2921.
[24] Arshad SN, Lach TG, Pouryazdan M, Hahn H, Bellon P, Dillon SJ, et al. Scripta Mater 2013;68:215.
[25] Cai W, Bellon P. Wear 2013;303:602.
[26] Rabinowicz E. Friction and wear of materials. New York: John Wiley & Sons; 1995.
[27] Archard JF. J Appl Phys 1953;24:981.
[28] Najafabadi R, Srolovitz DJ, Ma E, Atzmon M. J Appl Phys 1993;74:3144.
[29] Tian YZ, Wu SD, Zhang ZF, Figueiredo RB, Gao N, Langdon TG. Acta Mater 2011;59:2783.
[30] Pouryazdan M, Schwen D, Wang D, Scherer T, Hahn H, Averback RS, et al. Phys Rev B 2012;86:144302.
[31] Martin G. Ann Chim – Sci Mater 1981;6:46.
[32] Gente C, Oehring M, Bormann R. Phys Rev B 1993;48:13244.
[33] Wu F, Bellon P, Melmed AJ, Lusby TA. Acta Mater 2001;49:453.
[34] Zghal S, Hytch MJ, Chevalier JP, Twesten R, Wu F, Bellon P. Acta Mater 2002;50:4695.
[35] Ma E. Prog Mater Sci 2005;50:413.
[36] Odunuga S, Li Y, Krasnochtchekov P, Bellon P, Averback RS. Phys Rev Lett 2005;95:045901.
[37] Delogu F. J Appl Phys 2008;104:073533.
[38] Zhilyaev AP, Langdon TG. Prog Mater Sci 2008;53:893.
[39] Persson BNJ. Sliding friction: physical principles and applications. Berlin: Springer Verlag; 2000.
[40] Bellon P, Averback RS, Odunuga S, Li Y, Krasnochtchekov P, Caro A. Phys Rev Lett 2007;99:110602.
[41] Dautzenberg JH, Zaat JH. Wear 1973;23:9.
[42] Cai W, Bellon P. Acta Mater 2012;60:6673.
[43] Hughes DA, Chrzan DC, Liu Q, Hansen N. Phys Rev Lett 1998;81:4664.
[44] Hughes DA, Hansen N. Acta Mater 2000;48:2985.
[45] Hughes DA, Hansen N. Phys Rev Lett 2001;87:135503.
[46] Hughes DA. Scripta Mater 2002;47:697.
[47] Pantleon W. J Mater Res 2002;17:2433.
[48] Hansen N, Jensen DJ. Mater Sci Technol – Lond 2011;27:1229.
[49] Pantleon W. Mater Sci Forum 2011;667–669:205.
[50] Berdichevsky VL. J Mech Phys Solids 2012;60:1.
[51] Liu XC, Zhang HW, Lu K. Science 2013;342:337.

[52] Wen M, Cizek P, Wen C, Hodgson P, Li YC. Scripta Mater 2013;68:499.
[53] Muratore C, Voevodin AA. Annu Rev Mater Res 2009;39:297.
[54] Zheng S, Beyerlein IJ, Carpenter JS, Kang K, Wang J, Han W, et al. Nat Commun 2013;4:1696.
[55] Suresh S. Science 2001;292:2447.